How transposons drive evolution of virulence in a fungal pathogen

Luigi Faino[1#], Michael F Seidl[1#], Xiaoqian Shi-Kunne[1], Marc Pauper[1], Grardy CM van den Berg[1], Alexander HJ Wittenberg[2], and Bart PHJ Thomma[1]*

[1]Laboratory of Phytopathology, Wageningen University, Droevendaalsesteeg 1, 6708 PB Wageningen, The Netherlands

[2]Keygene N.V., Agro Business Park 90, 6708 PW Wageningen, The Netherlands

[#]These authors contributed equally to this work

*Corresponding author: Prof. dr. Bart PHJ Thomma
Chair, Laboratory of Phytopathology
Wageningen University
Droevendaalsesteeg 1
6708 PB Wageningen
The Netherlands
Email: bart.thomma@wur.nl

Running title: Genome evolution by transposable elements

Keywords: Genome evolution; Transposable element; Plant pathogen; *Verticillium dahliae*; segmental genome duplication

Abstract

Genomic plasticity enables adaptation to changing environments, which is especially relevant for pathogens that engage in arms races with their hosts. In many pathogens, genes mediating aggressiveness cluster in highly variable, transposon-rich, physically distinct genomic compartments. However, understanding of the evolution of these compartments, and the role of transposons therein, remains limited. We now show that transposons are the major driving force for adaptive genome evolution in the fungal plant pathogen *Verticillium dahliae*. Highly variable genomic regions evolved by frequent segmental duplications mediated by erroneous homologous recombination, often utilizing transposons, leading to genetic material that is free to diverge. Intriguingly, the duplicated regions are enriched in active transposons that further contribute to local genome plasticity. Thus, we provide evidence for genome shaping by transposons, both in an active and passive manner, which impacts the evolution of pathogen aggressiveness.

Introduction

Genomic plasticity enables organisms to adapt to environmental changes and occupy novel niches. While such adaptation occurs in any organism, it is particularly relevant for pathogens that engage in co-evolutionary arms races with their hosts (Raffaele and Kamoun 2012; Seidl and Thomma 2014; Dong et al. 2015). In these interactions, hosts utilize their surveillance system to detect invaders and mount appropriate defenses, which involves detection of invasion patterns by immune receptors, while pathogens secrete so-called effector molecules that support host colonization to counteract these immune responses (Rovenich et al. 2014; Cook et al. 2015). The tight interaction, in which the microbe tries to establish a symbiosis that the host tries to prevent, exerts strong selection pressure on both partners and incites rapid genomic diversification (McDonald and Linde 2002).

Sexual reproduction is an important mechanism to establish genotypic diversity by combining genetic information of two parental lineages, followed by meiotic recombination leading to novel combinations of existing alleles (McDonald and Linde 2002; de Visser and Elena 2007; Heitman 2010; Speijer et al. 2015). However, not all eukaryotes regularly reproduce sexually, including many fungal phyla that are thought to reproduce mainly asexually (Heitman et al. 2007; Flot et al. 2013). However, also in such asexual organisms adaptive genome evolution occurs, which is mediated by various mechanisms ranging from single-nucleotide polymorphisms to large-scale structural variations that can affect chromosomal shape, organization and gene content (Seidl and Thomma 2014). *Verticillium dahliae* is a soil-borne fungal pathogen that infects susceptible hosts through their roots and colonizes the water-conducting xylem vessels, leading to vascular wilt disease (Fradin and Thomma 2006). Despite its presumed asexual nature, *V. dahliae* is a highly successful pathogen that causes disease on hundreds of plant hosts (Fradin and Thomma 2006; Klosterman et al. 2009; Inderbitzin and Subbarao 2014). Verticillium wilt diseases are difficult to control due to the long viability of fungal resting structures in the soil, the broad host range of the pathogen, and inability of fungicides to eliminate the pathogen from infected xylem tissues. Moreover, little genetic resistance is available (Fradin and Thomma 2006). Thus,

63 novel methods for disease control are urgently required, which requires increased
64 understanding of the biology of the fungus in its interaction with host plants (Fradin and
65 Thomma 2006).

66 Using comparative genomics, we recently identified genomic rearrangements in *V.*
67 *dahliae* that lead to extensive chromosomal length polymorphisms between strains (de
68 Jonge et al. 2013). Moreover, the genomes of *V. dahliae* strains were found to contain highly
69 dynamic, repeat-rich regions that are only present in subsets of the *V. dahliae* population,
70 and thus have been referred to as lineage-specific (LS) (Klosterman et al. 2011; de Jonge et
71 al. 2013). Intriguingly, LS regions are enriched for *in planta*-induced effector genes that
72 contribute to fungal virulence (de Jonge et al. 2013). Therefore, it was hypothesized that
73 elevated genomic plasticity in LS regions contributes to diversification of effector repertoires
74 of *V. dahliae* lineages and thus mediates their aggressiveness (de Jonge et al. 2013; Seidl
75 and Thomma 2014). In a similar fashion, many filamentous pathogens evolved so-called
76 'two-speed' genomes with gene-rich, repeat-poor genomic compartments that contain core
77 genes that mediate general physiology and evolve slowly, whereas plastic, gene-poor and
78 repeat-rich compartments are enriched in effector genes that mediate aggressiveness in
79 interactions with host plants and evolve relatively quickly (Raffaele and Kamoun 2012).

80 Plastic, fast-evolving genomic compartments in plant and animal pathogen genomes
81 concern particular regions that are either embedded within the core chromosomes or reside
82 on conditionally dispensable chromosomes (Thon et al. 2006; Fedorova et al. 2008; Haas et
83 al. 2009; Ma et al. 2010; Goodwin et al. 2011; Klosterman et al. 2011; Rouxel et al. 2011; de
84 Jonge et al. 2013). Irrespective of the type of organization of the 'two-speed' genome, the
85 fast-evolving compartment is generally enriched for transposable elements (TEs). These
86 elements have been hypothesized to actively promote genomic changes by causing DNA
87 breaks during excision, or by acting as a substrate for rearrangement (Seidl and Thomma
88 2014). Nevertheless, the exact role of TEs in the evolution of effector genes currently
89 remains unknown, as well as the molecular mechanisms and the evolutionary trajectories
90 that govern genome plasticity (Dong et al. 2015). Thus far, in-depth studies of the precise

roles of TEs were hampered by fragmented pathogen genome assemblies caused by limitations in sequencing technologies, leading to poor assemblies of repeat-rich areas particularly (Faino et al. 2015; Thomma et al. 2015). We recently obtained gapless *V. dahliae* whole-genome assemblies using a combination of long-read sequencing and optical mapping (Faino et al. 2015). Here, we exploit these novel assemblies for in-depth investigation into the molecular mechanisms that are responsible for genomic variability, and are instrumental for adaptive genome evolution in the plant pathogen *V. dahliae*.

Results

Genomic rearrangements in Verticillium dahliae *are associated with extensive sequence similarity*

To investigate the molecular mechanisms that underlie genomic rearrangements in *V. dahliae*, we performed whole-genome alignments between strains JR2 and VdLs17 (Faino et al. 2015), revealing 24 synteny disruptions (Fig.1A; Supplemental Fig. 1). To further increase the resolution of these synteny breakpoints, we subsequently aligned long (average ~9 kb) sequencing reads derived from strain VdLs17 (Faino et al. 2015) to the completed, gapless assembly of *V. dahliae* stain JR2, and reads of which the two sides aligned to two distinct genomic locations were used to determine breakpoints at high-resolution (Supplemental Fig. 2). After manual refinement, this procedure yielded 19 large-scale chromosomal rearrangements, 13 of which concern inter-chromosomal translocations and 6 concern intra-chromosomal inversions (Fig. 1; Table 1). Of these 19 rearrangements, seven were confined to regions smaller than 100 bp (Table 1). The remaining 12 genomic rearrangements, in particular intra-chromosomal inversions, concern to larger genomic regions that could not be further refined due to the presence of strain-specific and/or repeat-rich regions (Fig. 1B).

We subsequently assessed the occurrence of the 13 inter-chromosomal rearrangements in nine other *V. dahliae* strains by querying paired-end reads derived from these genomes for pairs of discordantly mapped reads (i.e. both reads fail to map at the expected distance and/or location) when mapped onto the assembly of *V. dahliae* strain JR2 (Supplemental Fig. 3). This analysis revealed distinct rearrangement patterns among various strains (Supplemental Fig. 3B). For example, while some synteny breakpoints identified in *V. dahliae* strain JR2 are either specific to *V. dahliae* strain VdLs7 (Chr1: 2,843,014-2,843,020; Supplemental Fig. 4A) or common to all other *V. dahliae* strains (Chr1: 8,013,865-8,013,868; Supplemental Fig. 4B), some are observed in only a subset of *V. dahliae* strains (Chr3: 3,130,776-3,130,781; Supplemental Fig. 4C). Thus, genomic rearrangements commonly occur in different *V. dahliae* strains, suggesting a common mechanism driving their formation.

Genomic rearrangements are generally caused by double-strand DNA breakages followed by unfaithful repair by DNA repair mechanisms that utilize homologous sequences to repair such breaks (Hedges and Deininger 2007; Krejci et al. 2012; Seidl and Thomma 2014). Repetitive genomic elements, such as transposable elements (TEs), may give rise to genomic rearrangements by providing an ectopic substrate that interferes with faithful repair of the original break (Hedges and Deininger 2007; Seidl and Thomma 2014). Notably, out of 19 chromosomal rearrangements identified in *V. dahliae* strain JR2, 15 co-localize with a repetitive element (Table 1; Supplemental Table 1). However, even though genomic rearrangements in *V. dahliae* were previously associated with LTR-type retrotransposons (de Jonge et al. 2013), we were neither able to confirm this association nor systematically associate these structural variations to any other class of repetitive elements when using the completely assembled genomes of *V. dahliae* strains JR2 and VdLs17 (Faino et al. 2015) (Table 1). To understand the mechanisms that contributed to their formation, we studied the 13 inter-chromosomal rearrangements between *V. dahliae* strain JR2 and VdLs17 in more detail. Of these 13 rearrangements, 12 could be reconstructed in detail (Fig. 1B; Table 1; Supplemental Fig. 5). Eight of these 12 syntenic breakpoints occur over highly similar TEs in both strains, albeit that they belong to different TE families (Fig. 1C; Table 1; Supplemental Fig. 5). Closer inspection of the four remaining breakpoints revealed a TE at two of the breakpoints in *V. dahliae* strain VdLs17, while this TE was absent at those breakpoints in the JR2 strain. For the final two breakpoints no association to a TE was found in either strain, but extended sequence similarity surrounding the rearrangement site was identified (Fig. 1C). Therefore, we conclude that not necessarily TEs or their activity, but rather stretches of sequence similarity are associated with ectopic chromosomal rearrangements in *V. dahliae*, likely mediating unfaithful homology-based DNA repair. Since TEs are more abundant compared to other (types of) sequences, these are more likely to become substrate for double-strand repair pathways.

152 *Lineage-specific genomic regions in* Verticillium dahliae *evolved by segmental genomic*
153 *duplications*

154 Chromosomal rearrangements can lead to ectopic insertions, duplications or deletions of
155 genomic material, which play relevant roles in pathogen evolution during the arms race with
156 host plants (Seidl and Thomma 2014). Whole-genome alignments between *V. dahliae* strains
157 JR2 and VdLs17 revealed four large (>10 kb) repeat-rich genomic regions that do not display
158 synteny between the strains (Supplemental Fig. 6; Supplemental Table 2), suggesting that at
159 least part of the genomic material is absent in the respective other *V. dahliae* strain and
160 indicating extensive differential gene loss at these specific genomic locations. Moreover,
161 mapping of reads from nine additional strains (de Jonge et al. 2012) onto the JR2 and
162 VdLs17 assemblies revealed absence of read coverage mainly at their respective LS regions
163 (Supplemental Fig. 7). Notably, several inter-chromosomal rearrangements co-localize with
164 these LS regions (Fig. 1A), suggesting that genomic rearrangements contribute to the
165 formation of LS regions.

166 Chromosomal rearrangements not only lead to deletion of genetic material, e.g. in LS
167 regions (Fig. 1A), but also foster genomic duplications (Seidl and Thomma 2014). Even
168 though duplicated genes have previously been observed in LS regions of *V. dahliae*
169 (Klosterman et al. 2011), the extent of such duplications and their role in the evolution of LS
170 regions remains unknown. To determine the extent of segmental duplications in LS regions,
171 we employed two approaches. First, we performed whole-genome nucleotide alignments *of*
172 *V. dahliae* strain JR2 to itself to identify highly similar (>80% identity), large-scale duplication
173 events (Fig. 2A). Unanticipated, the vast majority of highly similar large-scale duplications
174 occurs within LS regions, while only very few of such duplications occur outside these
175 regions (Fig. 2A). Second, we performed homology detection between protein-coding genes
176 in *V. dahliae* strain JR2, establishing a set of ~1,000 paralogous sequences (Fig. 2B).
177 Notably, 40% of the 418 genes located in LS regions have a paralog (Fig. 2B), which is a
178 4.5x enrichment when compared to the core genome where only 7% of the ~11,000 genes

has a paralog (hypergeometic test; p = $1.31*10^{-69}$). Therefore, duplications of genomic material are instrumental for the constitution of LS regions in *V. dahliae* (Fig. 2B).

The high level of similarity between sequences located at LS regions (Fig. 2A) suggests that the duplications occurred rather recently. To firmly establish when these duplications occurred during the evolution of *V. dahliae*, we used the rate of synonymous substitutions per synonymous site (Ks) between paralogous gene pairs as a proxy for time since these sequences diverged (Fig. 2C). While the Ks distribution of paralogous pairs located in the core genome displays a single peak, indicating a single and distinct period in which the majority of these duplications occurred, the distribution of paralogous pairs where at least one gene is located in the LS regions displays two distinct peaks (Fig. 2C). Notably, the older of the two peaks coincides with the peak observed for the core paralogs (Fig. 2C), indicating that the expansion of core genes and a subset of genes in LS regions occurred in the same period. The additional peak points towards duplications that occurred more recently (Fig. 2C). To place these periods in relation to speciation events, we estimated Ks distributions for orthologous gene pairs between *V. dahliae* strain JR2 and a number of closely related fungi from the taxonomic class of Hypocreomycetidae (Fig. 2D). Within this group of close relatives, the tomato wilt pathogen *Fusarium oxysporum* f.sp. *lycopersici* was the first one to diverge from the last common ancestor, while the most recent split was the divergence of *V. dahliae* strains JR2 and VdLs17 (Fig. 2D). The first duplication period affected both the core genome and LS compartments, and occurred after the divergence of *F. oxysporum* f.sp. *lycopersici*, but before the divergence of *Colletotrichum higginsianum*, the causal agent of anthracnose leaf-spot disease of crucifers (Fig. 2D). Notably, all fungi that diverged after speciation of *F. oxysporum* f.sp. *lycopersici* display a peak in the Ks distribution for paralogous gene pairs at approximately the same period, although *A. alcalophilium* shows a less pronounced peak (Fig. 2D). The second duplication event in *V. dahliae* strain JR2 that specifically concerned genes located at LS regions occurred much more recently, after the speciation of *Verticillium alfalfae* (Fig. 2D). As it was previously shown that genes in the LS regions are particularly relevant for pathogen aggressiveness in

V. dahliae (de Jonge et al. 2013), this suggests that recent gene duplications are contributing to the evolution of aggressiveness.

The recent duplications that affected LS regions have generated raw genetic material that can be subject to subsequent rapid evolutionary diversification, leading to novel or altered gene functionality, but can also be subject to differential loss of one of the duplicated gene copies (Fig. 3A; Supplemental Fig. 8). In general, LS regions in *V. dahliae* strain JR2 display considerable gene loss, since for ~100 of the ~400 genes located in LS regions no ortholog could be detected in *V. dahliae* strain VdLs17. For example, a repeat-rich, ~100 kb LS region that contains ~20 genes that duplicated on chromosome 2 displays loss of multiple genes (Fig. 3A; Supplemental Fig. 8), a process that is similarly observed in VdLs17. Thus, differential gene loss significantly contributed to the diversification of LS regions. To determine if LS regions display signs of increased gene diversification and selection pressure acting on protein-coding genes, we used the rate of nonsynonymous substitutions per nonsynonymous site (Ka) as well as the ratio of Ka to Ks values calculated between orthologous gene pairs of *V. dahliae* strain JR2 and the closest related *Verticillium* species, *V. alfalfae*, as a proxy. Genes located at LS regions display moderately increased Ka values, as well as Ka/Ks values, when compared to genes residing in the core genome (median of 0.05 compared to 0.02, and 0.37 compared to 0.17, respectively). While these indicate accelerated sequence divergence of genes located within LS regions, the moderate differences also corroborate previous results (de Jonge et al. 2013; Seidl et al. 2015), suggesting that sequence divergence only plays a minor role in *V. dahliae* genome evolution.

The Ave1 *effector gene is located in a highly dynamic genomic region*

As shown above, highly dynamic LS regions are characterized by frequent gene duplications (Fig. 2), and by differential gene loss (Fig. 3; Supplemental Fig. 8). Moreover, effector genes located in LS regions play decisive roles in pathogen-host interactions (de Jonge et al. 2013). For example, Ave1 is an important LS effector that determines *V. dahliae* aggressiveness on various host plants (de Jonge et al. 2012). As expected in a co-evolutionary arms race

(Thomma et al. 2011; Cook et al. 2015), host recognition of this effector evolved as tomato plants that carry the immune receptor Ve1 recognize this effector to establish immunity (Fradin et al. 2009; de Jonge et al. 2012). Consequently, race 2 strains of *V. dahliae* lost *Ave1*, thus evading recognition by Ve1, leading to the capacity to infect *Ve1* tomato plants.

In *V. dahliae* strain JR2, *Ave1* is embedded in a gene-sparse and repeat-rich LS region on chromosome 5 (Fig. 3B-E; ~550,000-1,050,000). Notably, the average number of single nucleotide polymorphisms (SNPs) inferred from three race 1 and eight race 2 strains of *V. dahliae* is significantly reduced in the area surrounding the *Ave1* locus (between 680,000 and 720,000) when compared with the surrounding genomic regions (Fig. 3B), but also compared to genome-wide SNP levels in LS and core regions (Supplemental Fig. 9). As Ave1 is a strong contributor to virulence on plants lacking *Ve1* (de Jonge et al. 2012), selection pressure may drive the high level of conservation and lack of SNPs (Fig. 3B) in this region in race 1 strains.

Phylogenetic analyses revealed that *Ave1* was likely acquired by *V. dahliae* through horizontal gene transfer from plants (de Jonge et al. 2012). Intriguingly, however, *V. dahliae* race 1 strains do not occur as a monophyletic clade in the *V. dahliae* population (Supplemental Fig. 3A) (de Jonge et al. 2013), and thus it remains unclear how the *Ave1* locus distributed throughout the *V. dahliae* population. To assess if *Ave1* was gained or lost multiple times, we studied the genomic region surrounding the *Ave1* locus in the LS region. As expected, alignments of genome assemblies of multiple *V. dahliae* strains revealed the absence of *Ave1* in all race 2 strains (Supplemental Fig 10A). By mapping paired-end reads derived from genomic sequencing of various *V. dahliae* strains onto the genome assembly of *V. dahliae* strain JR2 we observed clear differences in coverage levels between *V. dahliae* race 1 and race 2 strains that carry or lack the *Ave1* gene, respectively (Fig. 3C; Supplemental Fig. 10B). While *V. dahliae* race 1 strains, including JR2, displayed an even level of read coverage over the *Ave1* locus, indicating that this region is similar in all race 1 stains, no read coverage of the *Ave1* gene was found for race 2 strains (Fig. 3C-D). Intriguingly, read coverage surrounding the *Ave1* gene revealed that race 2 strains can be

divided into three groups depending on the exact location of the read coverage drop (Fig. 3C). Whereas one group of isolates does not display any read coverage up to 720 kb, two groups display distinct regions in which the read coverage around the *Ave1* locus drops (Fig. 3C-E: red lines around 668 kb and green lines around 672 kb). Our finding strongly suggests that the *Ave1* locus was lost multiple times from the *V. dahliae* population, pointing to strong selection pressure posed by the Ve1 immune receptor on *V. dahliae* to lose *Ave1*. In conclusion, the *Ave1* locus is situated in a highly dynamic and repeat-rich region (Fig. 3C). Therefore, the most parsimonious evolutionary scenario is that the *Ave1* locus was horizontally acquired either directly or indirectly from plants once, followed by multiple losses in independent lineages that encountered host plants that carried Ve1 or functional homologs of this immune receptor (Thomma et al. 2011; de Jonge et al. 2012; Zhang et al. 2014). It is tempting to speculate that the transposable elements that flank the *Ave1* locus (Fig. 3C) contributed to the evolution of the *Ave1* locus by facilitating swift loss of the effector gene upon recognition by the Ve1 immune receptor.

Lineage-specific genomic regions in Verticillium dahliae *contain active transposable elements*

While the activity of TEs is not associated with the formation of extensive genome rearrangements, LS regions in *V. dahliae* are highly enriched for TEs, and their presence and potential activity may contribute to accelerated evolution of these genomic regions. In *V. dahliae*, the most abundant class of TEs are retrotransposons that transpose within the genome using an RNA intermediate (Wicker et al. 2007; Faino et al. 2015) (Supplemental Table 1). We assessed TE dynamics by querying the transcriptional activity of TEs using *in vitro* RNA-Seq data derived from *V. dahliae* strain JR2(de Jonge et al. 2012). Notably, the majority of TEs in *V. dahliae* are not transcribed and thus likely not active (Supplemental Table 1), while transcribed and therefore likely active TEs are found in LS regions (Supplemental Fig. 11).

To further assess if and how TEs influence the evolution of LS regions, we explored TE dynamics in the genome of *V. dahliae* strain JR2. Each copy of a TE in the genome is derived from an active ancestor that, once transposed and integrated into the genome, accumulates mutations that, over evolutionary time, will render the TE inactive. The relative age of individual TEs can thus be estimated based on sequence divergence from a consensus sequence that can be derived from present-day copies of any given TE. Using the Jukes-Cantor distance (Jukes and Cantor 1969), which corrects the divergence between TEs and their consensus sequence for multiple substitutions, we estimated the divergence times for TEs in the *V. dahliae* strain JR2 genome (Fig. 4). This analysis showed that TEs mainly transposed and expanded in two distinct periods (Fig. 4A). Notably, a considerable amount of 'younger' TEs, i.e. with small Jukes-Cantor distance to their consensus sequence, localizes in LS regions while the majority of 'older' TEs reside in the core genome (Fig. 4A). Next, we attempted to determine the relative period in which the majority of TEs in the genome of *V. dahliae* strain JR2 transposed. To this end, we derived Jukes-Cantor distributions for orthologous genes of *V. dahliae* strain JR2 and individual closely related fungi as a proxy of divergence between these species (Fig. 4C). These distributions display the same pattern of species divergence when derived from phylogenetic analyses (Supplemental Fig. 12) as well as from the Ks distributions between orthologous gene pairs (Fig. 2D). By comparing the Jukes-Cantor distributions derived from TEs and from orthologous genes, we revealed that 'older' TEs transposed around the separation of *V. dahliae* and *V. alfalfa*, while the 'younger' TEs transposed after *V. dahliae* speciation (Fig. 4C). Notably, 'younger' TEs tend to be transcriptionally active, while 'older', more diverged TEs tend to be transcriptionally silent (Fig. 4B). Thus, the expansion of younger TEs is recent and mainly concerns the active TEs localized at LS regions (Fig. 4), strongly suggesting that TE-transpositions contribute to the genetic plasticity of LS regions.

Discussion

Many plant pathogens contain a so-called 'two-speed' genome where effector genes reside in genomic compartments that are considerably more plastic than the core of the genome, facilitating the swift evolution of effector catalogs that are required to be competitive in the host-pathogen arms race (Raffaele and Kamoun 2012; Dong et al. 2015). Generally, effector compartments are enriched in transposable elements (TEs), and it has been speculated that they promote genomic flexibility and drive accelerated evolution of these genomic compartments (Gijzen 2009; Haas et al. 2009; Ma et al. 2010; Raffaele et al. 2010; Rouxel et al. 2011; Raffaele and Kamoun 2012; de Jonge et al. 2013; Wicker et al. 2013; Grandaubert et al. 2014; Seidl and Thomma 2014; van Hooff et al. 2014; Dong et al. 2015; Faino et al. 2015; Seidl et al. 2015). Nevertheless, the exact role of TEs in the evolution of effector genes, as well as the molecular mechanisms and the evolutionary trajectories that govern the formation of the 'two-speed' genome, and the corresponding local genome plasticity, remained unknown (Raffaele and Kamoun 2012; Dong et al. 2015). Here, we studied the evolution of the 'two-speed' genome of the vascular wilt pathogen *V. dahliae*, which was significantly facilitated by the recent establishment of gapless whole-genome assemblies of two highly similar *V. dahliae* strains that, despite their high (>99%) degree of sequence identity, display severe genomic rearrangements (Faino et al. 2015; Thomma et al. 2015). We identified ~2 Mb repeat-rich, lineage-specific (LS) regions between the two *V. dahliae* strains (Fig. 1; Supplemental Fig. 6-7) that are significantly enriched in TEs and contain all thus far functionally analyzed effector genes, including *Ave1* (Fig. 3C) (de Jonge et al. 2012; de Jonge et al. 2013). Moreover, we also determined a significant number of synteny breakpoints that are associated with genomic rearrangements to high resolution, and we were able to reconstitute most of the rearrangements in detail (Fig. 1; Table 1; Supplemental Fig. 5). Previously, we showed a strong association between LS compartments and the occurrence of genomic rearrangements (de Jonge et al. 2013). Even though this correlation was overestimated due to significant errors in the publically available genome assembly of *V. dahliae* strain VdLs17 (Klosterman et al. 2011) for which we later revealed a considerable

number of erroneous chromosomal inversions (Faino et al. 2015) (Table 1), we nevertheless observed that three out of four large-scale LS regions are associated with chromosomal rearrangements (Fig. 1), corroborating that chromosomal rearrangements significantly contribute to the evolution of LS regions in *V. dahliae*. We were not able to associate every LS region with a genomic rearrangement (Fig. 1), like we were also not able to exactly reconstitute each genomic rearrangement (Fig. 1; Supplemental Fig. 5). However, it can easily be anticipated that complex rearrangements occurred in which genetic material in close proximity was lost. Furthermore, likely these rearrangements (continuously) occurred over longer evolutionary timescales (Supplemental Fig. 3; Supplemental Fig. 4), and subsequent rearrangement events may have erased 'scars' of previous rearrangements. Thus, even though not every genomic rearrangement leads to a new LS region, large-scale genomic alterations are the driving force for their formation in *V. dahliae*.

Genomic rearrangements can lead to a multitude of structural variations, including translocations, duplications and gene loss (Seidl and Thomma 2014). Here, we show that the LS compartments of *V. dahliae* strain JR2 evolved by frequent segmental duplications that yielded genetic material that subsequently obtained the freedom to diverge (Fig. 2B). Intriguingly, these duplications occurred recently, namely after divergence of *V. dahliae* and *V. alfalfae* (Fig. 2). However, this is not the only wave of duplications that shaped the *V. dahliae* genome, as an earlier duplication period was found that concerns duplications found in the core genome (Fig. 2). Notably, this duplication event was not only observed in *V. dahliae*, but also in related species including *V. alfalfae*, *V. albo-atrum*, *A. alcalophilium* and *C. higginsianum*, yet not in *F. oxysporum*, suggesting that this duplication occurred after the speciation of *F. oxysporum* from the last common ancestor of the more recently evolved fungi (Fig. 2). Given the high abundance of duplicated genes at a confined point in evolution, it is tempting to speculate that a single genome-wide event, for example a whole-genome duplication or hybridization, gave rise to these duplicates. Potentially, this particular duplication event determined that, despite their similar life style and physiology, *V. dahliae* evolved LS regions that are embedded within its core genome, while *F. oxysporum* evolved

LS genetic material as conditionally dispensable chromosomes that can be horizontally transferred (Ma et al. 2010).

Based on our data, which indicate that TEs can be implicated in many yet not all genomic rearrangements, it is conceivable that homologous recombination using TE sequences as a substrate, rather than TE activity, is responsible for the establishment of gross rearrangements. In this manner, TEs have passively contributed to the genome evolution of *V. dahliae*, and to the extensive genomic plasticity that can be observed between *V. dahliae* strains (Fig. 1). In addition to the passive roles of TE in genome evolution, we also obtained evidence for the involvement of TE activity in the evolution of *V. dahliae*. Intriguingly, while the majority of TEs in *V. dahliae* is transcriptionally silent and thus inactive, transcriptionally active and thus actively transposing TEs were observed in LS regions (Fig. 4, Supplemental Fig. 9). Similarly, transcription and specific induction of TE activity has been observed previously in *V. dahliae* strain VdLs17 (Amyotte et al. 2012). These independent observations are further corroborated by our dating analyses suggesting that TEs that localize in LS regions are significantly 'younger' when compared with those residing in the core genome (Fig. 4). Active transposition can contribute to genome plasticity by causing gene deletions at their target sites. Moreover, TEs in proximity of genes can also profoundly influence their expression, as shown for the barley smut fungus *Ustilago hordei* where a TE insertion in the promoter of the *UhAvr1* effector changed its expression, leading to loss of host recognition (Ali et al. 2014). Interestingly, frequent gene loss is observed within the segmental duplications that constitute the LS regions (Fig. 2; Supplemental Fig. 8). Similarly, the LS effector *Ave1* is located in an LS region (Fig. 3) with several transposable elements (TE) in its direct vicinity (de Jonge et al. 2012) (Fig. 3C), and clear evidence for repeated loss in the *V. dahliae* population was obtained in our study. Although based on our data these transposons cannot directly be implicated in the acquisition of *Ave1* from plants, they likely facilitated the multiple losses of *Ave1* that are observed in independent lineages incited by selection pressure posed by the *Ve1* resistance gene of tomato, or functional homologs that may occur in other plants (Fradin et al. 2009; Thomma et al. 2011; de Jonge et al. 2012;

399 Zhang et al. 2013). However, although *Ave1* resides in a LS region, and LS regions are
400 characterized by the presence of active TEs, it remains unclear whether the frequent loss of
401 *Ave1* is actually mediated by TE activity. It has similarly been hypothesized that ectopic
402 genomic rearrangements caused by homology-based DNA repair pathways, possibly
403 passively mediated by TEs, drive the frequent loss of the *Avr-Pita* effector gene in isolates of
404 the rice blast fungus *Magnaporthe oryzae* that encountered the *Pita* resistance gene of rice
405 (Orbach et al. 2000; Chuma et al. 2011). Similar processes likely contribute to the frequent
406 recovery of *Avr-Pita* in *M. oryzae* strains relieved from selection pressure of Pita, leading to
407 translocation and duplications of this effector gene in dynamic genomic regions (Chuma et al.
408 2011).

409 Genome-wide studies in several fungi aiming to study chromatin – the complex of
410 DNA and proteins - revealed that TE-rich regions are generally associated to highly
411 condensed chromatin, the so-called heterochromatin, that restricts transcription and TE
412 activity (Lewis et al. 2009; Connolly et al. 2013; Galazka and Freitag 2014). Therefore, TEs
413 can influence the expression of neighboring genes such as effectors, as they can direct the
414 formation of heterochromatic regions (Lewis et al. 2009). In the saprophytic fungus
415 *Neurospora crassa*, heterochromatin formation at TEs is directed by remnants of Repeat
416 Induced Point mutations (RIP), a pre-meiotic process that actively induces point mutations in
417 TEs (Selker 1990; Lewis et al. 2009; Lewis et al. 2010). In the pathogenic fungus
418 *Leptosphaeria maculans*, effectors are located in TE-rich regions that were subjected to
419 extensive RIP mutations (Rouxel et al. 2011). Notably, effectors within these regions display
420 signatures of nucleotide mutations caused by the RIP process, fostering rapid effector
421 diversification (Fudal et al. 2009; Daverdin et al. 2012). LS regions in *V. dahliae* are TE-rich
422 and effector genes are directly flanked by TEs (de Jonge et al. 2012; de Jonge et al. 2013;
423 Seidl et al. 2015)(Fig. 3). Only few transposable elements in *V. dahliae* display typical RIP
424 mutations, which might indicate that *V. dahliae* possessed an active RIP mechanism
425 (Klosterman et al. 2011; Amyotte et al. 2012), likely connected to sexual cycle, in its
426 evolutionary past. However, all currently known *V. dahliae* strains, but also other *Verticillium*

427 species have been described as asexual and therefore RIP is no longer likely to occur. *V.*
428 *dahliae* effectors in LS regions do not display evidence for RIP mutations that could
429 contribute to effector diversification or to formation of heterochromatic regions. Despite the
430 fact that LS regions do not show overrepresentation of secreted genes, we previously
431 observed that effector genes residing in the LS regions are considerably overrepresented in
432 the *V. dahliae* transcriptome upon plant infection (de Jonge et al. 2013). In the present study,
433 we highlight that TEs that reside in LS regions are relatively young and several are
434 transcriptionally active. Therefore, we hypothesize that these regions, in contrast to the core
435 genomic compartments, are either not yet targeted by heterochromatin formation or carry
436 different chromatin marks, or that LS regions represent facultative heterochromatin that can
437 dynamically change its conformation, thereby influencing DNA accessibility and thus effector
438 gene expression. For example, in the soybean pathogen *Phytophthora sojae* expression of
439 the effector *Avr3a* is repressed by chromatin-based mechanism (Qutob et al. 2013; Gijzen et
440 al. 2014). Suppression of effector expression leads to avoidance of recognition by the host
441 surveillance system, yet allows for swift effector recovery and activation on susceptible hosts
442 (Gijzen 2009; Qutob et al. 2013). Chromatin-based regulation of effector genes and genes
443 encoding other virulence factors has been observed in several pathogenic fungi (Connolly et
444 al. 2013; Qutob et al. 2013; Chujo and Scott 2014; Soyer et al. 2014; Soyer et al. 2015). This
445 suggests that facultative heterochromatin located in dynamic compartments of the two-speed
446 genome, e.g. LS regions in *V. dahliae*, is pivotal to regulate effector and virulence gene
447 expression.

448 Chromosome condensation of heterochromatic regions supposedly restricts genomic
449 rearrangements (Galazka and Freitag 2014), yet these regions in the plant pathogens
450 *Fusarium graminearum* are enriched for genomic rearrangements (Connolly et al. 2013). In
451 *V. dahliae*, LS regions are formed by recent duplications and harbor active TEs, suggesting
452 that these regions are susceptible to structural variation such as genomic rearrangements. A
453 recent study in yeasts and mammals suggests that genomic rearrangements occur between
454 open chromatin in regions that are in close proximity within the nucleus (Berthelot et al.

455 2015). Moreover, this study concludes that genomic rearrangements between TEs alone are
456 not sufficient to fully explain the rearrangements that were observed (Berthelot et al. 2015).
457 Expression of clustered virulence genes in the human malaria pathogen *Plasmodium*
458 *falciparum* is tightly regulated by chromatin and, even though these virulence clusters are
459 located on different chromosomes, they co-localize in close proximity within the nucleus (Ay
460 et al. 2014). Even though these co-localized clusters have been associated with condensed,
461 and thus repressive chromatin, extensive ectopic chromosomal rearrangements between
462 clusters have been observed (Freitas-Junior et al. 2000; Lopez-Rubio et al. 2009; Jiang et al.
463 2013; Ay et al. 2014), suggesting that the chromatin structure plays roles in their evolution. In
464 fungi, however, co-localization of effector genes in the nucleus has not yet been reported.
465 Based on initial work in other eukaryotes, we conceive that complex chromatin structures in
466 pathogenic fungi will not only influence coordinated effector expression in LS regions, but
467 also genomic rearrangements, thereby further linking genome and chromatin structure to
468 genome evolution. Thus, further insight into chromatin biology of plant pathogens will be
469 instrumental to significantly accelerate our knowledge on the evolution of the ‘two-speed’
470 genome, and on fungal aggressiveness.

Methods

Genome annotation and dynamics

Gene predictions for the whole-genome assembly of *V. dahliae* strain JR2(Faino et al. 2015) was performed using the Maker2 software (Holt and Yandell 2011). To this end, RNA-seq reads derived from different *in vitro* and *in planta* conditions(de Jonge et al. 2012) were mapped to the genome using Tophat2 (default settings) (Trapnell et al. 2009). Additionally, gene sequences derived from previous genome annotations as well as protein sequences from 35 fungal proteomes were used as additional evidence (Klosterman et al. 2011; de Jonge et al. 2013; Seidl et al. 2015).

Homology between 13 fungal species was assessed using OrthoMCL (default settings)(Li et al. 2003). Sequence similarity between proteins was established by all-vs.-all analyses using BLASTp (E-value cutoff 1e-5, soft filtering)(Altschul et al. 1990). Ks values between gene pairs, as defined by OrthoMCL families, were calculated using the Nei-Gojobori algorithm included in the KaKs_Calculator 2.0 package(Wang et al. 2010). The coding sequences of gene pairs were aligned using protein alignment as a guide. The phylogenetic tree was generated by RAxML(Stamatakis 2006) using concatenated protein sequences of 3,492 single-copy orthologs that are conserved among eight fungal species, where only a single representative species was chosen for the fungal genera *Colletotrichum* and *Fusarium* (Supplemental Fig. 12).

Repetitive elements were identified as described in Faino et al. (2015). Briefly, repetitive elements were identified using RepeatScout, LTR_Finder and LTRharvest, and the repetitive elements identified by the different software were combined (non-redundant). Repetitive elements were further classified as described by Wicker et al. (2007). Open reading frames within the transposable elements were identified by BlastN and BlastX (Camacho et al. 2009) searches against NCBI NR databases as well as by InterProScan (Jones et al. 2014). Repetitive elements that could not be classified were defined as 'unknown'. Expression of repetitive elements was assessed based on RNA sequencing data derived from *V. dahliae* strain JR2 grown in *in vitro* media (Czapek Dox) (de Jonge et al.

2012). Single reads were mapped onto the genome assembly of *V. dahliae* strain JR2 using Tophat2 (default parameters) (Trapnell et al. 2009). Mapped reads were summarized using the R package GenomicAlignments ('summarizeOverlaps') (Lawrence et al. 2013), and the expression per repetitive element, excluding simple repeats and repeats overlapping genes, as well as per gene was reported as Reads Per Kilobase of transcript per Million mapped reads (RPKM).

To estimate divergence time of transposable elements, each individual copy of a transposable element was aligned to the consensus of its family using needle, which is part of the EMBOSS package (Rice et al. 2000). The consensus sequence for each transposable element family was determined by performing multiple-sequence alignment of all copies belonging to the same family using mafft (Katoh and Standley 2013) (each individual copy needed to be longer than 400 bp). For the consensus sequence, only columns with > 1 aligned sequence (excluding gaps) were considered, for which the nucleotide occurring in the majority of sequences was used for the consensus sequence (ties, a nucleotide randomly chosen from the tie was picked). The sequence divergence between transposable elements and the consensus was corrected using the Jukes-Cantor distance, which corrects the divergence (p) by the formula $d=-3/4\log_e(1-4/3p)$(Jukes and Cantor 1969).

Identification of genomic rearrangements

Whole-genome alignments between chromosomes of the genome assemblies of *V. dahliae* strains JR2 and VdLS17(Faino et al. 2015) were performed using nucmer (default settings), which is part of the MUMmer 3.0 package(Kurtz et al. 2004). To remove spurious hits, the alignments were subsequently filtered by length, retaining alignments > 15 kb and 99% identity. These parameters were chosen based on the average nucleotide identity between the two *V. dahliae* strains (99.98%), as well as the average length of unique sequences in the genome. These whole-genome alignments were further mined for genomic rearrangements and associated synteny breakpoints in *V. dahliae* strain JR2. The identified synteny breakpoints were further refined by mapping PacBio long-sequencing reads derived

by genomic sequencing of *V. dahliae* strain VdLS17 to the genome of *V. dahliae* strain JR2 using Blasr (default settings) (Chaisson and Tesler 2012), followed by manual refinement. GEvo (Lyons et al. 2008) was used to identify syntenic regions between *V. dahliae* strains JR2 and VdLs17, where only gene-coding regions were used as anchors between the syntenic chromosomal regions.

To assess the presence or absence of genomic rearrangements in other *V. dahliae* strains, paired-end reads derived from genome sequencing (de Jonge et al. 2012) were mapped onto the genome of *V. dahliae* strain JR2 using BWA (BWA-mem algorithm) (Li and Durbin 2010). Genomic regions surrounding the identified genomic rearrangements (± 4 kb) were visually evaluated for the quantity of concordantly and discordantly mapped reads as well as orphan reads.

Identification and analyses of highly dynamic genomic regions

Whole-genome alignments between chromosomes of the complete genome assemblies of *V. dahliae* strains JR2 and VdLS17 (Faino et al. 2015) were performed using nucmer (settings: -maxmatch), which is part of the MUMmer 3.0 package (Kurtz et al. 2004). Alignments separated by gaps <500 bp were merged in unique and contiguous alignments. LS regions were manually defined by identifying regions accumulating alignments breaks and TEs. Additionally, genomic reads derived from ten *V. dahliae* strains (de Jonge et al. 2012) were mapped on the *V. dahliae* strain JR2 and VdLs17, respectively, using Bowtie2 (default settings) (Langmead et al. 2009). The genomic coverage was determined by BEDtools (Quinlan and Hall 2010). The phylogenetic tree of eleven different *V. dahliae* strains was generated using RealPhy (Bertels et al. 2014) using either *V. dahliae* strain JR2 or VdLs17 as a reference strain.

The presence/absence analysis of the *Ave1* locus was performed by aligning paired-end reads from DNA sequencing of eleven *V. dahliae* strains (de Jonge et al. 2012) (including JR2) to the assembled genome of *V. dahliae* strain JR2 using BWA (BWA-mem algorithm) (Li and Durbin 2010). We averaged the raw read depth per genomic position in

genomic windows (window-size 5 kb; slide 500 bp (Figure 3D; E) and window-size 500 bp; slide 100 bp (Supplemental Fig 10B), respectively), and subsequently performed a G+C correction similarly as previously described (Yoon et al. 2009). Briefly, we adjusted these averaged raw read depth (ARD) based on the observed deviation of read depth for a given G+C percentage. To this end, we first determined the average ARD for G+C percentages ranging from 0-100% (by 1%). Subsequently, we corrected the ARD using the formula $ARDc_i = ARD_i * (m/m_{G+C})$, where $ARDc_i$ is the corrected ARD in the *i*th window, ARD_i is the ARD in the *i*th window, m is the average ARD over all windows, and m_{G+C} is the average ARD for all windows with the same G+C percentage as the *i*th window (Yoon et al. 2009). Additionally, the genomic reads of each individual additional *V. dahliae* strain were assembled using A5 pipeline (v.20140113) (Tritt et al. 2012). The assembled genomes were aligned to the genome assembly of *V. dahliae* strain JR2 genome using nucmer (settings: -maxmatch), which is part of the MUMmer 3.0 package (Kurtz et al. 2004). Overlaps between genomic coordinates of different genome features, e.g. lineage-specific regions, genes or transposable elements, were assessed by BEDtools (v2.24.0) (Quinlan and Hall 2010) or by the R package GenomicRanges (Lawrence et al. 2013).

Single nucleotide polymorphisms (SNPs) were identified using GATK v2.8.1 (DePristo et al. 2011). Briefly, paired-end reads derived from ten *V. dahliae* strains(de Jonge et al. 2012) were mapped onto the complete genome assembly of *V. dahliae* strain JR2 (Faino et al. 2015) using BWA (BWA-mem algorithm) (Li and Durbin 2010). Using GATK v2.8.1 (DePristo et al. 2011), mapped reads were locally realigned to minimize the number of mismatches over all reads, and subsequently genomic variants (SNPs) were called using GATK's UnifiedGenotyper (default settings; emitting threshold 20, haploid organism) and resulting variants were quality filtered (quality > 50; phred-scaled quality score for the assertion), depth > 10 and allelic frequency > 0.9). SNPs derived from different strains were summarized in non-overlapping windows of 1 kb, and the number of SNPs derived from the individual strains were averaged per window. Absence of a SNP in a particular strain was only considered if the corresponding position displayed read coverage.

583 **Data access**

584 The genome assemblies of *V. dahliae* strain JR2 and VdLS17 are available from NCBI under
585 the assembly number GCA_000400815.2 and GCA_000952015.1, respectively (Faino et al.
586 2015). Paired-end reads derived from genomic sequencing of *V. dahliae* strains as well as
587 RNA sequencing reads were generated by de Jonge et al. (2012) (PRJNA169154). Genome
588 sequences and annotation for *Fusarium oxysporum* f. sp. *lycopersici*, *Colletotrichum*
589 *higginsianum* were retrieved from the Ensembl fungi database (http://fungi.ensembl.org/).
590 The data for *Acremonium alcalophilum* were downloaded from JGI database, and the data
591 for *V. alfalfa* MS102 (Klosterman et al. 2011) were obtained from the *Verticillium* database at
592 the Broad Institute.

593

594 **Acknowledgments**

595 Work in the laboratory of BPHJT is support by the Research Council Earth and Life Sciences
596 (ALW) of the Netherlands Organization of Scientific Research (NWO). MFS acknowledges
597 the receipt of a VENI grant of ALW-NWO, project number 863.15.005.

598

599 **Author Contributions**

600 LF conceived the study, participated in its design and coordination, performed analyses, and
601 contributed to writing of the manuscript; MFS conceived the study, participated in its design
602 and coordination, performed analyses, and wrote the manuscript; GCMB produced biological
603 materials used in the study; XSK and MP performed analyses; AHJW participated in the
604 establishment of high-quality genome assemblies; BPHJT conceived the study, participated
605 in its design and coordination, and wrote the manuscript. All authors read and approved the
606 final manuscript.

607

608 **Competing Financial Interests**

609 A.H.J.W. is a full-time employee of KeyGene N.V., a company offering next-generation
610 sequencing services, including PacBio sequencing. The remaining authors declare no
611 competing financial interests.

612 **Figure Legends**

613 **Figure 1 – Extensive rearrangements in *Verticillium dahliae* genomes are mediated by**
614 **repetitive elements.** (A) Syntenic regions, indicated by ribbons, between chromosomes of
615 the two highly similar *V. dahliae* strains JR2 (chromosomes displayed in white) and VdLs17
616 (chromosomes displayed in grey) reveal multiple synteny breakpoints caused by inter-
617 chromosomal rearrangements, highlighted by red arrows for the JR2 genome. Red bars on
618 the chromosomes indicate lineage-specific genomic regions (LS) that lack synteny in the
619 other strain. To facilitate visibility, some chromosomes of *V. dahliae* strain VdLs17 have been
620 reversed and complemented (indicated by asterisks). (B) Synteny blocks displayed on the
621 chromosomes of *V. dahliae* strain JR2 colored based on synteny with VdLs17 chromosomes.
622 LS regions are shown in white and indicate loss of synteny. (C) Detailed view of the genomic
623 regions surrounding five synteny breakpoints that are highlighted by boxes in (b).
624 Rearrangements over short homologous regions such as repetitive elements (black boxes)
625 or genes (colored boxes) resulted in inter-chromosomal rearrangements (translocations). *V.*
626 *dahliae* strain VdLs17 genes were inferred by mapping of the *V. dahliae* strain JR2 genes to
627 the genome assembly of *V. dahliae* strain VdLs17. Dashed grey lines indicate rearrangement
628 sites.

629

630 **Figure 2 - Whole-genome alignments of *Verticillium dahliae* strain JR2 reveals two**
631 **duplication events**. (A) Circos diagram illustrating sequence alignments within *V. dahliae*
632 strain JR2. Black lines indicate genomic regions with sequence similarity. The inner circle
633 shows LS regions (red lines), the middle circle indicates clusters of LS regions and the outer
634 circle shows the identity between pairs of secondary alignments. Each cluster of LS region is
635 colour coded: LS1 in blue, LS2 in yellow, LS3 in brown and LS4 in light blue (see Table S2).
636 (B) Circos diagram illustrating paralogous gene pairs in *V. dahliae* strain JR2. Paralogous
637 gene pairs of which at least one member is located at the LS regions are connected with blue
638 lines, while paralogous gene pairs located in the core genome are connected with red lines.
639 (C) Ks distribution of paralogs of which both genes are located in the core genome (red) or at

640 least one paralogs is located in an LS region (blue). (D) Duplication events are estimated by
641 calculating the Ks value for paralogous gene pairs and displayed in the line graph. Speciation
642 events are estimated by calculating the Ks value for orthologous gene pairs based on genes
643 from *V. dahliae* strains JR2 and their respective orthologs in the other genomes and
644 displayed in the box plot. Distributions and median divergence times between orthologous
645 pairs, displayed by box plots, were used to estimate relative speciation events.
646
647 **Figure 3 – Gene loss after segmental duplications within the *V. dahliae* strain JR2**
648 **genome.** (A) Example of a segmental duplication between LS regions located on
649 chromosome 2. Red ribbons indicate regions of homology between the two loci. Blue arrows
650 indicate gene models present only at one of the two loci while green and red arrows indicate
651 common genes and transposable elements, respectively. (B) Single nucleotide
652 polymorphism (SNP) density (mean number of SNPs per 1 kb) over the *Ave1* locus indicates
653 depletion of SNPs in the *Ave1* region when compared with neighboring regions. (C) A large
654 genomic region on chromosome 5 of *V. dahliae* strain JR2 containing the *Ave1* gene (red
655 box) is characterized by presence/absence polymorphisms between strains. Lines indicate
656 the corrected average read depth (per 5 kb window, 500 bp slide) of paired-end reads
657 derived from genomic sequencing of eleven *V. dahliae* strains. Different colors indicate
658 distinct patterns of coverage across the *Ave1* locus. Genes and transposable
659 elements/repeats (excluding simple repeats) are indicated. (D) Magnification in of the *Ave1*
660 locus, highlighting the four dominating coverage patterns. (E) Detailed view of paired-end
661 reads derived from *V. dahliae* strains VdLs17 and St100, revealing distinct regions where the
662 sequence coverage drops.
663
664 **Figure 4 – Dynamics of transposable elements in the genome of *Verticillium dahliae***
665 **strain JR2.** (A) The divergence time of transposable elements identified in the genome of *V.*
666 *dahliae* strain JR2 (Faino et al. 2015) was estimated using the Jukes-Cantor distance
667 calculated between repeat copies and their consensus sequence. The distributions of

668 divergence times between transposable elements located in the core genome (red) and in
669 the LS regions (blue) differ. Estimations of speciation events in the evolutionary history of *V.*
670 *dahliae* are indicated by triangles based on analyses in (C). (B) The distributions of
671 divergence times between expressed/active ($\log_{10}$ (RPKM+1) ≥ 1) transposable elements
672 (red) and non-expressed (blue) transposable elements differ. Estimations of speciation
673 events are indicated by triangles. (C) Speciation evens are estimated by calculating the
674 Jukes-Cantor distance for orthologous gene pairs based on genes from *V. dahliae* strains
675 JR2 and their respective orthologs in the other genomes. Distributions and median
676 divergence times between orthologous pairs, displayed by box plots, were used to estimate
677 relative speciation events.

678 **Figures**

679

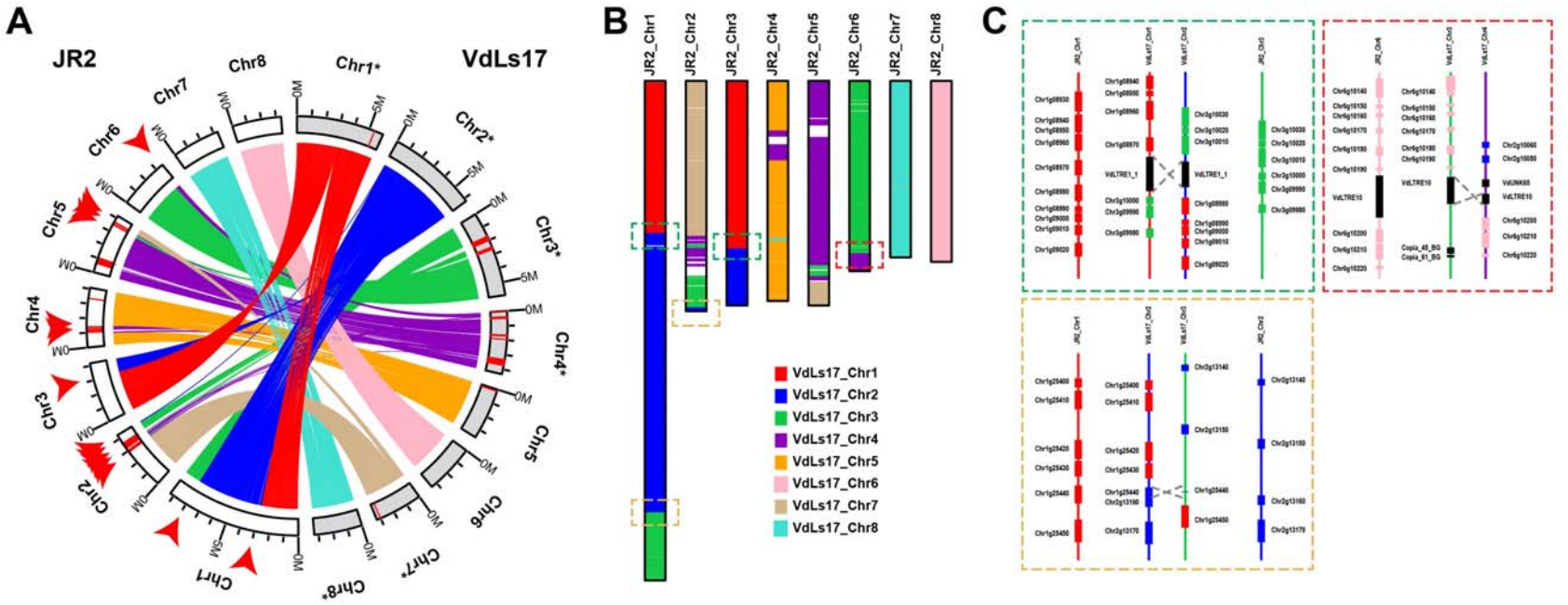

680

681 **Figure 1**

682

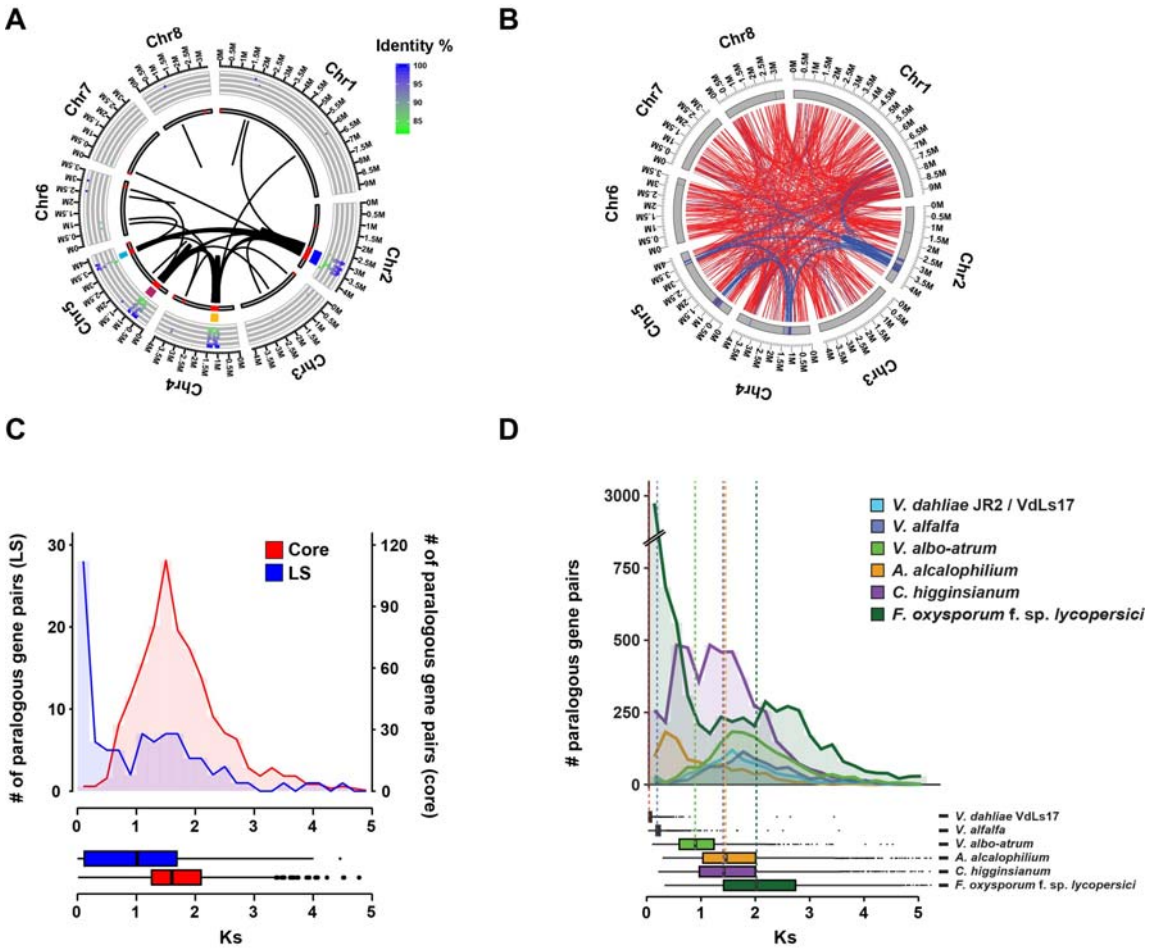

Figure 2

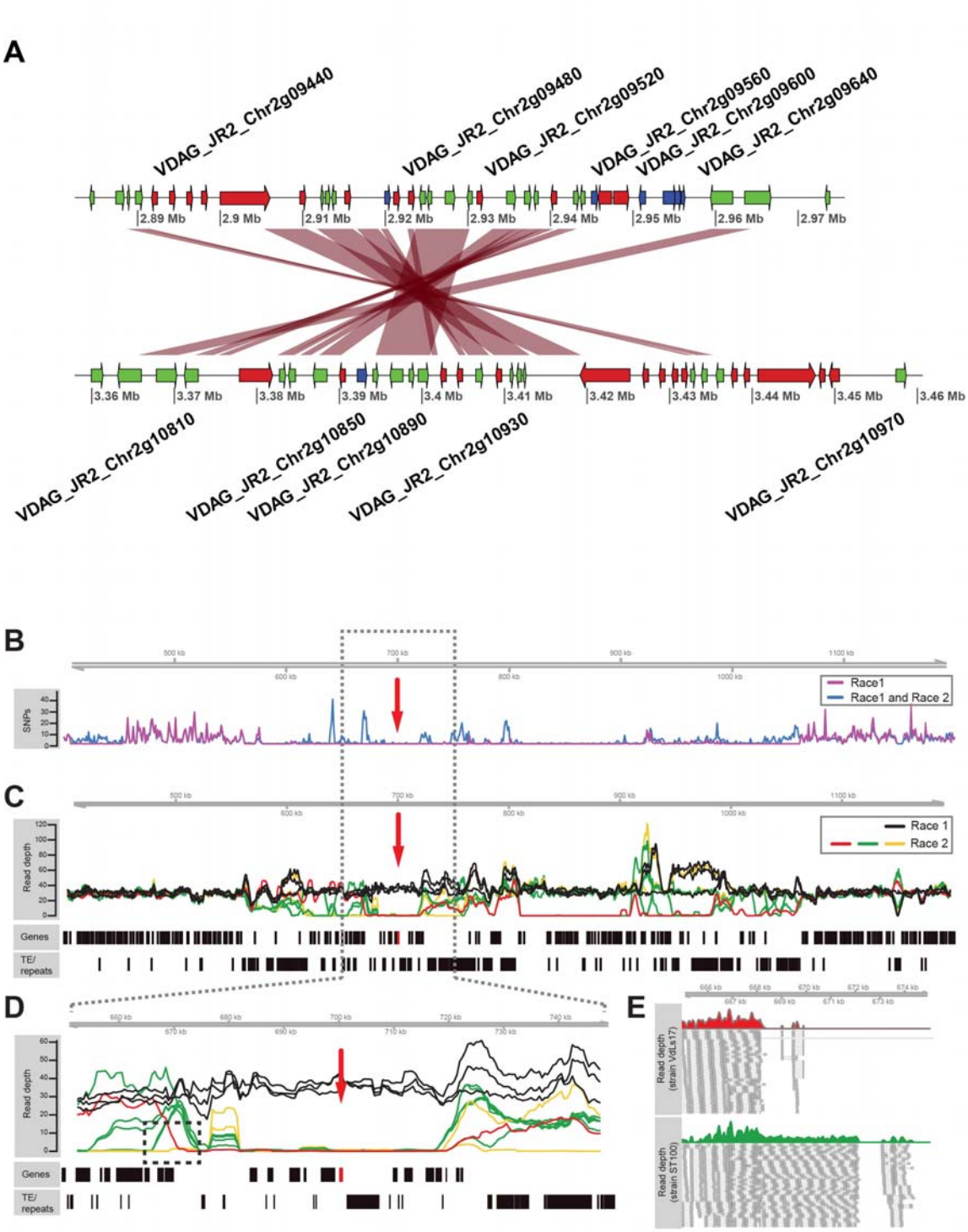

687

688 **Figure 3**

689

690 **Figure 4**

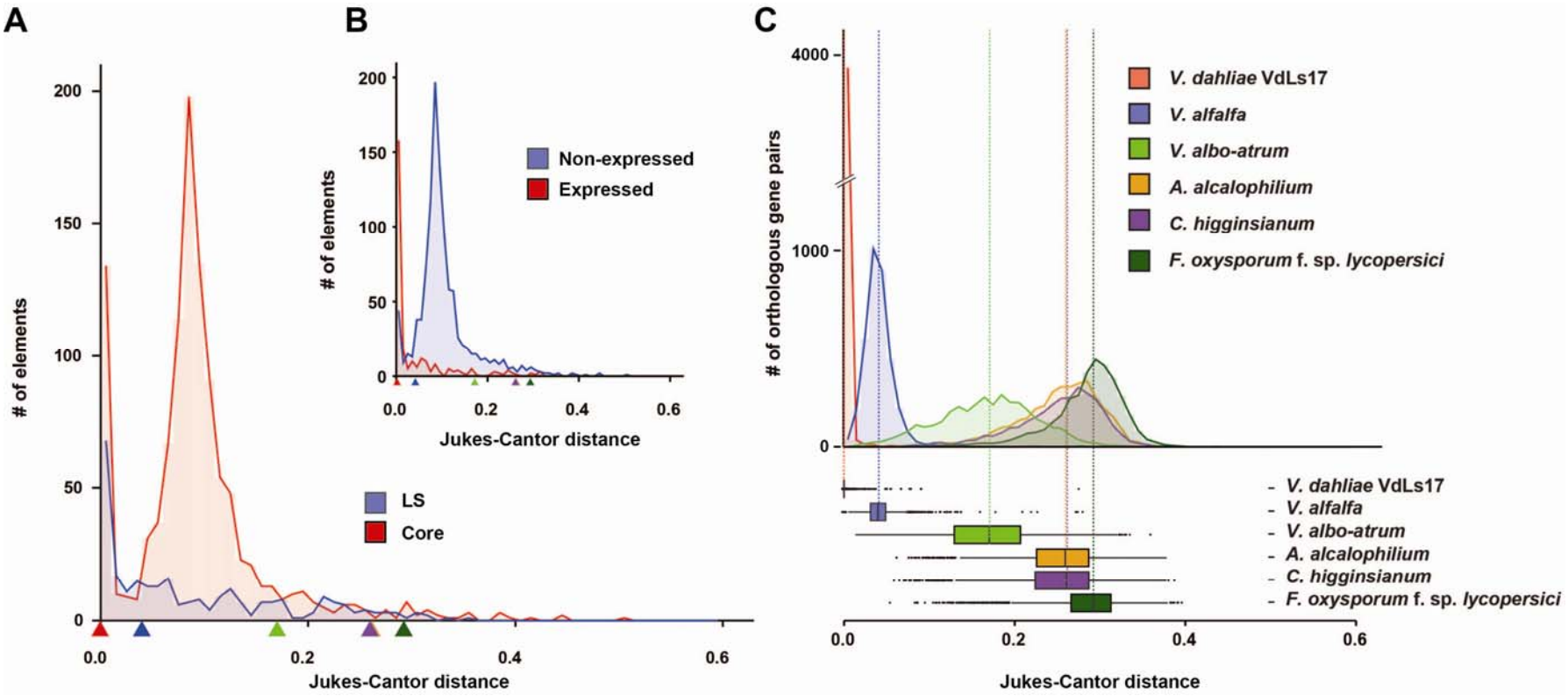

691

692

693 **Tables**

694 **Table 1**: Genomic location of synteny breakpoints identified in *Verticillium dahliae* strain JR2 and the closest flanking genomic element.

Chr.	Synteny break point *				Flanking genomic element					
	Start	End	Interval (bp)	Type**	Start	End	Strand	Genomic element***	Distance to breakpoint (bp)	Index****
Chr1	2,843,014	2,843,020	6	TRA#	2,840,162	2,843,030	+	VDAG_JR2_Chr1g08970	0	a
Chr1	7,140,631	7,162,273	21,643	INV	7,162,232	7,162,992	+	VdLTRE8	0	
Chr1	7,227,694	7,243,623	15,930	INV	7,242,070	7,248,997	+	VdLTRE12	0	
Chr1	8,013,865	8,013,868	3	TRA#	8,013,244	8,014,018	-	VDAG_JR2_Chr1g25440	0	b
Chr2	2,876,424	2,897,525	21,102	TRA	2,896,858	2,898,045	+	VdUNK31	0	c
Chr2	3,025,499	3,031,900	6,401	TRA	3,032,060	3,032,744	-	VdLTRE8	166	d
Chr2	3,120,447	3,122,897	2,451	TRA	3,122,730	3,124,038	+	VdUNK65	0	e
Chr2	3,334,994	3,620,790	285,796	TRA	3,620,790	3,629,961	-	VdLTRE10	0	f
Chr2	4,225,478	4,225,575	97	TRA#	4,225,210	4,226,425	-	VDAG_JR2_Chr2g13160	0	b
Chr3	149,893	166,205	16,313	INV	164,460	166,293	+	VdUNK19	0	
Chr3	226,642	226,647	5	INV	225,927	226,658	+	VdLTRE8	0	
Chr3	3,130,776	3,130,781	5	TRA#	3,129,525	3,130,711	-	VDAG_JR2_Chr3g10000	45	a
Chr4	1,464,458	1,480,146	15,689	TRA	1,479,722	1,479,771	+	5SrRNA-1_BG	0	
Chr5	2,171,284	2,202,070	30,787	INV	2,195,136	2,202,070	+	VdLTRE2_1	0	
Chr5	2,367,806	2,390,749	22,944	INV	2,390,710	2,390,856	+	VdUNK100	0	
Chr5	3,423,150	3,423,640	491	TRA	3,422,285	3,423,644	+	VdLTRE12	0	d
Chr5	3,642,999	3,644,451	1,453	TRA	3,644,182	3,650,054	+	VdLTRE1_1	0	f
Chr5	3,686,406	3,686,412	6	TRA	3,685,349	3,686,592	-	VdUNK11	0	c
Chr6	3,218,241	3,218,279	39	TRA#	3,212,527	3,220,016	+	VdLTRE10	0	e

695 [*]Location of synteny breakpoints are determined by comparison between *Verticillium dahliae* strains JR2 and VdLS17.

696 [**]Synteny breakpoints are classified as inter-chromosomal translocation (TRA) or as intra-chromosomal inversion (INV). Rearrangement events

697 labelled with [#] are graphically displayed in Figure 1C.

698 [***]The closest genomic elements comprise genes and repeats (see also Supplementary Table 2).

699 [****]The letter label in the last column (Index) indicates the panel in Supplementary Fig. 5 in which the particular rearrangement is graphically

700 displayed.

References

Ali S, Laurie JD, Linning R, Cervantes-Chavez JA, Gaudet D, Bakkeren G. 2014. An immunity-tiggering effector from the barley smut fungus *Ustilago hordei* resides in an Ustilaginaceae-specific cluster bearing signs of transposable element-assisted evolution. *PLoS Path* **10**: e1004223.

Altschul SF, Gish W, Miller W, Myers EW, Lipman DJ. 1990. Basic local alignment search tool. *J Mol Biol* **215**: 403-410.

Amyotte SG, Tan XP, Pennerman K, Jimenez-Gasco MD, Klosterman SJ, Ma LJ, Dobinson KF, Veronese P. 2012. Transposable elements in phytopathogenic *Verticillium* spp.: insights into genome evolution and inter- and intra-specific diversification. *BMC Genomics* **13**: 314.

Ay F, Bunnik EM, Varoquaux N, Bol SM, Prudhomme J, Vert JP, Noble WS, Le Roch KG. 2014. Three-dimensional modeling of the *P. falciparum* genome during the erythrocytic cycle reveals a strong connection between genome architecture and gene expression. *Genome Res* **24**: 974-988.

Bertels F, Silander OK, Pachkov M, Rainey PB, van Nimwegen E. 2014. Automated reconstruction of whole-genome phylogenies from short-sequence reads. *Mol Biol Evol* **31**: 1077-1088.

Berthelot C, Muffato M, Abecassis J, Crollius HR. 2015. The 3D organization of chromatin explains evolutionary fragile genomic regions. *Cell Rep* **10**: 1913-1924.

Camacho C, Coulouris G, Avagyan V, Ma N, Papadopoulos J, Bealer K, Madden TL. 2009. BLAST plus : architecture and applications. *BMC Bioinformatics* **10**: 421.

Chaisson MJ, Tesler G. 2012. Mapping single molecule sequencing reads using basic local alignment with successive refinement (BLASR): application and theory. *BMC Bioinformatics* **13**: 238.

Chujo T, Scott B. 2014. Histone H3K9 and H3K27 methylation regulates fungal alkaloid biosynthesis in a fungal endophyte-plant symbiosis. *Mol Microbiol* **92**: 413-434.

728 Chuma I, Isobe C, Hotta Y, Ibaragi K, Futamata N, Kusaba M, Yoshida K, Terauchi R,
729 Fujita Y, Nakayashiki H et al. 2011. Multiple translocation of the *AVR-Pita* effector gene
730 among chromosomes of the rice blast fungus *Magnaporthe oryzae* and related species.
731 *PLoS Path* **7**: e1002147.
732 Connolly LR, Smith KM, Freitag M. 2013. The *Fusarium graminearum* histone H3K27
733 methyltransferase KMT6 regulates development and expression of secondary metabolite
734 gene clusters. *PLoS Genet* **9**: e1003916.
735 Cook DE, Mesarich CH, Thomma BPHJ. 2015. Understanding plant immunity as a
736 surveillance system to detect invasion. *Annu Rev Phytopathol* **53**: 541-563.
737 Daverdin G, Rouxel T, Gout L, Aubertot JN, Fudal I, Meyer M, Parlange F, Carpezat J,
738 Balesdent MH. 2012. Genome structure and reproductive behaviour influence the
739 evolutionary potential of a fungal phytopathogen. *PLoS Pathog* **8**: e1003020.
740 de Jonge R, Bolton MD, Kombrink A, van den Berg GC, Yadeta KA, Thomma BPHJ.
741 2013. Extensive chromosomal reshuffling drives evolution of virulence in an asexual
742 pathogen. *Genome Res* **23**: 1271-1282.
743 de Jonge R, van Esse HP, Maruthachalam K, Bolton MD, Santhanam P, Saber MK,
744 Zhang Z, Usami T, Lievens B, Subbarao KV et al. 2012. Tomato immune receptor Ve1
745 recognizes effector of multiple fungal pathogens uncovered by genome and RNA
746 sequencing. *Proc Natl Acad Sci USA* **109**: 5110-5115.
747 de Visser JAG, Elena SF. 2007. The evolution of sex: empirical insights into the roles of
748 epistasis and drift. *Nature Reviews Genetics* **8**: 139-149.
749 DePristo MA, Banks E, Poplin R, Garimella KV, Maguire JR, Hartl C, Philippakis AA, del
750 Angel G, Rivas MA, Hanna M et al. 2011. A framework for variation discovery and
751 genotyping using next-generation DNA sequencing data. *Nat Genet* **43**: 491-498.
752 Dong S, Raffaele S, Kamoun S. 2015. The two-speed genomes of filamentous pathogens:
753 waltz with plants. *Curr Opin Genet Dev* **35**: 57-65.

754 Faino L, Seidl MF, Datema E, van den Berg GCM, Janssen A, Wittenberg AHJ, Thomma
755 BPHJ. 2015. Single-Molecule Real-Time sequencing combined with optical mapping yields
756 completely finished fungal genomes. *mBIO* **6**: e00936-00915.
757 Fedorova ND, Khaldi N, Joardar VS, Maiti R, Amedeo P, Anderson MJ, Crabtree J, Silva
758 JC, Badger JH, Albarraq A et al. 2008. Genomic islands in the pathogenic filamentous fungus
759 *Aspergillus fumigatus*. *PLoS Genet* **4**: e1000046.
760 Flot J-F, Hespeels B, Li X, Noel B, Arkhipova I, Danchin EG, Hejnol A, Henrissat B,
761 Koszul R, Aury J-M. 2013. Genomic evidence for ameiotic evolution in the bdelloid rotifer
762 *Adineta vaga*. *Nature* **500**: 453-457.
763 Fradin EF, Thomma BPHJ. 2006. Physiology and molecular aspects of Verticillium wilt
764 diseases caused by *V. dahliae* and *V. albo-atrum*. *Mol Plant Pathol* **7**: 71-86.
765 Fradin EF, Zhang Z, Ayala JCJ, Castroverde CDM, Nazar RN, Robb J, Liu CM, Thomma
766 BPHJ. 2009. Genetic dissection of Verticillium wilt resistance mediated by tomato *Ve1*. *Plant*
767 *Physiol* **150**: 320-332.
768 Freitas-Junior LH, Bottius E, Pirrit LA, Deitsch KW, Scheidig C, Guinet F, Nehrbass U,
769 Wellems TE, Scherf A. 2000. Frequent ectopic recombination of virulence factor genes in
770 telomeric chromosome clusters of *P. falciparum*. *Nature* **407**: 1018-1022.
771 Fudal I, Ross S, Brun H, Besnard AL, Ermel M, Kuhn ML, Balesdent MH, Rouxel T. 2009.
772 Repeat-induced point mutation (RIP) as an alternative mechanism of evolution toward
773 virulence in *Leptosphaeria maculans*. *Molecular plant-microbe interactions : MPMI* **22**: 932-
774 941.
775 Galazka JM, Freitag M. 2014. Variability of chromosome structure in pathogenic fungi - of
776 'ends and odds'. *Curr Opin Microbiol* **20**: 19-26.
777 Gijzen M. 2009. Runaway repeats force expansion of the *Phytophthora infestans* genome.
778 *Genome Biology* **10**: 241.
779 Gijzen M, Ishmael C, Shrestha SD. 2014. Epigenetic control of effectors in plant
780 pathogens. *Front Plant Sci* **5**.

781 Goodwin SB, M'Barek S B, Dhillon B, Wittenberg AH, Crane CF, Hane JK, Foster AJ, Van
782 der Lee TA, Grimwood J, Aerts A et al. 2011. Finished genome of the fungal wheat pathogen
783 *Mycosphaerella graminicola* reveals dispensome structure, chromosome plasticity, and
784 stealth pathogenesis. *PLoS Genet* **7**: e1002070.
785 Grandaubert J, Lowe RG, Soyer JL, Schoch CL, Van de Wouw AP, Fudal I, Robbertse B,
786 Lapalu N, Links MG, Ollivier B et al. 2014. Transposable element-assisted evolution and
787 adaptation to host plant within the *Leptosphaeria maculans-Leptosphaeria biglobosa* species
788 complex of fungal pathogens. *BMC Genomics* **15**: 891.
789 Haas BJ, Kamoun S, Zody MC, Jiang RH, Handsaker RE, Cano LM, Grabherr M, Kodira
790 CD, Raffaele S, Torto-Alalibo T et al. 2009. Genome sequence and analysis of the Irish
791 potato famine pathogen *Phytophthora infestans*. *Nature* **461**: 393-398.
792 Hedges DJ, Deininger PL. 2007. Inviting instability: Transposable elements, double-strand
793 breaks, and the maintenance of genome integrity. *Mutat Res* **616**: 46-59.
794 Heitman J. 2010. Evolution of eukaryotic microbial pathogens via covert sexual
795 reproduction. *Cell host & microbe* **8**: 86-99.
796 Heitman J, Kronstad JW, Taylor JW, Casselton L. 2007. *Sex in Fungi: Molecular*
797 *Determination and Evolutionary Implications*. ASM Press.
798 Holt C, Yandell M. 2011. MAKER2: an annotation pipeline and genome-database
799 management tool for second-generation genome projects. *BMC Bioinformatics* **12**: 491.
800 Inderbitzin P, Subbarao KV. 2014. *Verticillium* systematics and evolution: how confusion
801 impedes Verticillium wilt management and how to resolve it. *Phytopathology* **104**: 564-574.
802 Jiang LB, Mu JB, Zhang QF, Ni T, Srinivasan P, Rayavara K, Yang WJ, Turner L,
803 Lavstsen T, Theander TG et al. 2013. PfSETvs methylation of histone H3K36 represses
804 virulence genes in *Plasmodium falciparum*. *Nature* **499**: 223-227.
805 Jones P, Binns D, Chang HY, Fraser M, Li W, McAnulla C, McWilliam H, Maslen J,
806 Mitchell A, Nuka G et al. 2014. InterProScan 5: genome-scale protein function classification.
807 *Bioinformatics* **30**: 1236-1240.

Jukes TH, Cantor CR. 1969. Evolution of protein molecules. *Mammalian protein metabolism* **3**: 21-132.

Katoh K, Standley DM. 2013. MAFFT multiple sequence alignment software version 7: improvements in performance and usability. *Mol Biol Evol* **30**: 772-780.

Klosterman SJ, Atallah ZK, Vallad GE, Subbarao KV. 2009. Diversity, pathogenicity and management of *Verticillium* species. *Annu Rev Phytopathol* **47**: 39-62.

Klosterman SJ, Subbarao KV, Kang S, Veronese P, Gold SE, Thomma BPHJ, Chen Z, Henrissat B, Lee YH, Park J et al. 2011. Comparative genomics yields insights into niche adaptation of plant vascular wilt pathogens. *PLoS Path* **7**: e1002137.

Krejci L, Altmannova V, Spirek M, Zhao X. 2012. Homologous recombination and its regulation. *Nucleic Acids Res* **40**: 5795-5818.

Kurtz S, Phillippy A, Delcher AL, Smoot M, Shumway M, Antonescu C, Salzberg SL. 2004. Versatile and open software for comparing large genomes. *Genome Biology* **5**: R12.

Langmead B, Trapnell C, Pop M, Salzberg SL. 2009. Ultrafast and memory-efficient alignment of short DNA sequences to the human genome. *Genome Biology* **10**: R25.

Lawrence M, Huber W, Pages H, Aboyoun P, Carlson M, Gentleman R, Morgan MT, Carey VJ. 2013. Software for computing and annotating genomic ranges. *PLoS Comp Biol* **9**: e1003118.

Lewis ZA, Adhvaryu KK, Honda S, Shiver AL, Knip M, Sack R, Selker EU. 2010. DNA methylation and normal chromosome behavior in Neurospora depend on five components of a histone methyltransferase complex, DCDC. *PLoS Genet* **6**: e1001196.

Lewis ZA, Honda S, Khlafallah TK, Jeffress JK, Freitag M, Mohn F, Schubeler D, Selker EU. 2009. Relics of repeat-induced point mutation direct heterochromatin formation in *Neurospora crassa*. *Genome Res* **19**: 427-437.

Li H, Durbin R. 2010. Fast and accurate long-read alignment with Burrows-Wheeler transform. *Bioinformatics* **26**: 589-595.

Li L, Stoeckert CJ, Jr., Roos DS. 2003. OrthoMCL: identification of ortholog groups for eukaryotic genomes. *Genome Res* **13**: 2178-2189.

836 Lopez-Rubio J-J, Mancio-Silva L, Scherf A. 2009. Genome-wide analysis of
837 heterochromatin associates clonally variant gene regulation with perinuclear repressive
838 centers in malaria parasites. *Cell host & microbe* **5**: 179-190.
839 Lyons E, Pedersen B, Kane J, Alam M, Ming R, Tang HB, Wang XY, Bowers J, Paterson
840 A, Lisch D et al. 2008. Finding and Comparing Syntenic Regions among *Arabidopsis* and the
841 Outgroups Papaya, Poplar, and Grape: CoGe with Rosids. *Plant Physiol* **148**: 1772-1781.
842 Ma LJ, van der Does HC, Borkovich KA, Coleman JJ, Daboussi MJ, Di Pietro A, Dufresne
843 M, Freitag M, Grabherr M, Henrissat B et al. 2010. Comparative genomics reveals mobile
844 pathogenicity chromosomes in *Fusarium*. *Nature* **464**: 367-373.
845 McDonald BA, Linde C. 2002. Pathogen population genetics, evolutionary potential, and
846 durable resistance. *Annu Rev Phytopathol* **40**: 349-379.
847 Orbach MJ, Farrall L, Sweigard JA, Chumley FG, Valent B. 2000. A telomeric avirulence
848 gene determines efficacy for the rice blast resistance gene *Pi-ta*. *Plant Cell* **12**: 2019-2032.
849 Quinlan AR, Hall IM. 2010. BEDTools: a flexible suite of utilities for comparing genomic
850 features. *Bioinformatics* **26**: 841-842.
851 Qutob D, Chapman BP, Gijzen M. 2013. Transgenerational gene silencing causes gain of
852 virulence in a plant pathogen. *Nature Commun* **4**: 1349.
853 Raffaele S, Farrer RA, Cano LM, Studholme DJ, MacLean D, Thines M, Jiang RH, Zody
854 MC, Kunjeti SG, Donofrio NM et al. 2010. Genome evolution following host jumps in the Irish
855 potato famine pathogen lineage. *Science* **330**: 1540-1543.
856 Raffaele S, Kamoun S. 2012. Genome evolution in filamentous plant pathogens: why
857 bigger can be better. *Nature reviews Microbiology* **10**: 417-430.
858 Rice P, Longden I, Bleasby A. 2000. EMBOSS: The European molecular biology open
859 software suite. *Trends Genet* **16**: 276-277.
860 Rouxel T, Grandaubert J, Hane JK, Hoede C, van de Wouw AP, Couloux A, Dominguez
861 V, Anthouard V, Bally P, Bourras S et al. 2011. Effector diversification within compartments
862 of the *Leptosphaeria maculans* genome affected by Repeat-Induced Point mutations. *Nature*
863 *Commun* **2**: 202.

Rovenich H, Boshoven JC, Thomma BPHJ. 2014. Filamentous pathogen effector functions: of pathogens, hosts and microbiomes. *Curr Opin Plant Biol* **20C**: 96-103.

Seidl MF, Faino L, Shi-Kunne X, van den Berg GC, Bolton MD, Thomma BPHJ. 2015. The genome of the saprophytic fungus *Verticillium tricorpus* reveals a complex effector repertoire resembling that of its pathogenic relatives. *Mol Plant-Microbe Interact* **28**: 362-373.

Seidl MF, Thomma BPHJ. 2014. Sex or no sex: evolutionary adaptation occurs regardless. *Bioessays* **36**: 335-345.

Selker EU. 1990. Premeiotic instability of repeated sequences in *Neurospora crassa*. *Annu Rev Genet* **24**: 579-613.

Soyer JL, El Ghalid M, Glaser N, Ollivier B, Linglin J, Grandaubert J, Balesdent MH, Connolly LR, Freitag M, Rouxel T et al. 2014. Epigenetic control of effector gene expression in the plant pathogenic fungus *Leptosphaeria maculans*. *PLoS Genet* **10**: e1004227.

Soyer JL, Rouxel T, Fudal I. 2015. Chromatin-based control of effector gene expression in plant-associated fungi. *Curr Opin Plant Biol* **26**: 51-56.

Speijer D, Lukes J, Elias M. 2015. Sex is a ubiquitous, ancient, and inherent attribute of eukaryotic life. *Proc Natl Acad Sci USA* **112**: 8827-8834.

Stamatakis A. 2006. RAxML-VI-HPC: maximum likelihood-based phylogenetic analyses with thousands of taxa and mixed models. *Bioinformatics* **22**: 2688-2690.

Thomma BPHJ, Nurnberger T, Joosten MH. 2011. Of PAMPs and effectors: the blurred PTI-ETI dichotomy. *Plant Cell* **23**: 4-15.

Thomma BPHJ, Seidl MF, Shi-Kunne X, Cook DE, Bolton MD, van Kan JA, Faino L. 2015. Mind the gap; seven reasons to close fragmented genome assemblies. *Fungal Genet Biol* doi:10.1016/j.fgb.2015.08.010.

Thon MR, Pan H, Diener S, Papalas J, Taro A, Mitchell TK, Dean RA. 2006. The role of transposable element clusters in genome evolution and loss of synteny in the rice blast fungus *Magnaporthe oryzae*. *Genome biology* **7**: R16.

Trapnell C, Pachter L, Salzberg SL. 2009. TopHat: discovering splice junctions with RNA-Seq. *Bioinformatics* **25**: 1105-1111.

892 Tritt A, Eisen JA, Facciotti MT, Darling AE. 2012. An integrated pipeline for de novo
893 assembly of microbial genomes. *PloS one* **7**: e42304.
894 van Hooff JJ, Snel B, Seidl MF. 2014. Small homologous blocks in *Phytophthora* genomes
895 do not point to an ancient whole-genome duplication. *Genome Biol Evol* **6**: 1079-1085.
896 Wang D, Zhang Y, Zhang Z, Zhu J, Yu J. 2010. KaKs_Calculator 2.0: a toolkit
897 incorporating gamma-series methods and sliding window strategies. *Genomics Proteomics*
898 *Bioinformatics* **8**: 77-80.
899 Wicker T, Oberhaensli S, Parlange F, Buchmann JP, Shatalina M, Roffler S, Ben-David R,
900 Dolezel J, Simkova H, Schulze-Lefert P et al. 2013. The wheat powdery mildew genome
901 shows the unique evolution of an obligate biotroph. *Nat Genet* **45**: 1092-1096.
902 Wicker T, Sabot F, Hua-Van A, Bennetzen JL, Capy P, Chalhoub B, Flavell A, Leroy P,
903 Morgante M, Panaud O et al. 2007. A unified classification system for eukaryotic
904 transposable elements. *Nature Reviews Genetics* **8**: 973-982.
905 Yoon ST, Xuan ZY, Makarov V, Ye K, Sebat J. 2009. Sensitive and accurate detection of
906 copy number variants using read depth of coverage. *Genome Res* **19**: 1586-1592.
907 Zhang Z, Esse HP, Damme M, Fradin EF, Liu CM, Thomma BPHJ. 2013. Ve1-mediated
908 resistance against *Verticillium* does not involve a hypersensitive response in *Arabidopsis*.
909 *Mol Plant Pathol* **14**: 719-727.
910 Zhang Z, Song Y, Liu CM, Thomma BPHJ. 2014. Mutational analysis of the Ve1 immune
911 receptor that mediates *Verticillium* resistance in tomato. *PloS one* **9**: e99511.
912